The Astrophysical Journal, 677:683–691, 2008 April 10

UV AND RADIO OBSERVATIONS OF THE CORONAL SHOCK ASSOCIATED WITH THE 2002 JULY 23 CORONAL MASS EJECTION EVENT

S. Mancuso
Istituto Nazionale di Astrofisica, Osservatorio Astronomico di Torino, Strada Osservatorio 20, 10025 Pino Torinese, Torino, Italy; mancuso@oato.inaf.it

and

D. Avetta
Universitá di Torino, Via Giuria 1, 10125 Torino, Italy
Received 2007 September 6; accepted 2007 December 14

ABSTRACT

We report on the analysis of a fast coronal mass ejection (CME)–driven shock observed on 2002 July 23 with the Ultraviolet Coronagraph Spectrometer (UVCS) on board the *Solar and Heliospheric Observatory* (*SOHO*). The CME was first detected in white light by the Large Angle and Spectrometric Coronagraph Experiment (LASCO), and shock-associated type II metric emission was recorded by several ground-based radio spectrographs. The evolution of the excess broadening of the O VI λ1032 line profiles observed by UVCS at 1.63 $R_\odot$ is consistent with the passage of a CME-driven shock surface enveloping a bubble-type, conically expanding CME, and its dynamics is found to be well associated with the complex, multiple type II radio emission detected in the metric band. Our results suggest that there might be a deficiency of ion heating in the present event with respect to what was observed in previous CME shocks detected by UVCS, and that this paucity might be attributed to different local plasma conditions, such as higher ambient coronal plasma β. We conclude that plasma β could be an important parameter in determining the effect of ion heating at collisionless shock fronts in the solar corona.

Subject headings: line: profiles — shock waves — Sun: coronal mass ejections (CMEs) — Sun: radio radiation

1. INTRODUCTION

Coronal mass ejections (CMEs) with speeds in excess of the ambient magnetosonic speed eventually drive shocks ahead of them as they propagate away from the Sun. Shock waves generated by CMEs accelerate electron beams to suprathermal energies, which in turn can produce Langmuir waves that are converted by means of nonlinear wave-wave interactions into electromagnetic type II radio waves near the fundamental of the local electron plasma frequency $f_{\rm pe} \approx 9(n_e)^{1/2}$ kHz and its harmonic, where n_e is the electron density in cm^{-3} (see Gopalswamy [2006] for a recent review on the topic). Since the coronal density decreases with increasing heliocentric distance, the expanding shock surface will produce type II radio emission at decreasing frequencies as it propagates through space, and the measured frequency drift rate at a given time is directly related to the shock speed. The observed frequency drift rate, therefore, provides information on the shock dynamics through the corona, while its onset depends on the local Alfvén speed, which is governed by both the magnetic field and the plasma density (e.g., Lin et al. 2006). Both observations and theories suggest that type II radio emission is generated just upstream of the CME-driven shock (Cairns 1986; Bale et al. 1999; Knock et al. 2001), so that it should refer to unshocked plasma rather than to shocked (or CME) material. In a few cases, however, type II emission appears to be split into two parallel lanes separated by a few megahertz. This band splitting is interpreted as plasma emission occurring both upstream and downstream of the coronal shock front (Smerd et al. 1975; Vršnak et al. 2002; Cho et al. 2007).

Direct imaging of coronal shocks remains an outstanding observational challenge. While some features of CMEs observed in the corona in Thomson-scattered white light have been interpreted as signatures of shocks (Sime & Hundhausen 1987; Vourlidas et al. 2003), it is generally difficult to differentiate between hot, shock-compressed plasma and coronal ejecta such as loops and prominence material. Clear signatures of shock formation in the corona have been observed in the ultraviolet by Raymond et al. (2000), Mancuso et al. (2002), Raouafi et al. (2004), and Ciaravella et al. (2005) with the Ultraviolet Coronagraph Spectrometer (UVCS; Kohl et al. 1995) on board the *Solar and Heliospheric Observatory* (*SOHO*). Shock signatures along the UVCS slit were identified by wide and sudden broadening of the O VI spectral line profiles, together with simultaneous brightening of the spectral lines from heavier ions, and were found to be temporally associated with type II metric emission.

UVCS observations of the 2002 July 23 CME have already been analyzed by Raymond et al. (2003). The event was included in a study of three fast CME events that showed rarely observed transient brightenings in the [Fe XVIII] spectral line. During the CME passage, the O VI line profiles of two of the reported events (2002 April 21 and August 24) were clearly split into relatively narrow but strongly redshifted and blueshifted components. The absence of associated line broadening was interpreted as an indication of the lack of strong shock heating, possibly due to local fast-mode speeds faster than the CMEs. Although included in the above study, the 2002 July 23 CME event did not display a clear split into narrow redshifted and blueshifted components. In fact, Raymond et al. (2003) acknowledged, while discussing the origin of the observed [Fe XVIII] line emission, that a shock interpretation was still possible, in principle, at least for this event. The argument, however, lacked evidence, and the topic was not discussed further.

According to the spectra recorded by several ground-based radio observatories, strong type II signatures were detected on 2002 July 23 at the time corresponding to the CME passage through the UVCS slit. Since the whole CME leading-edge surface crossed

the slit, as will be shown later, the shock, if CME-driven, *must* have been passed *somewhere* along the slit and *should* have been observed by the UVCS. In this paper, by analyzing the UV spectra during the CME passage and the metric radio dynamic spectrum associated with this event, along with proper modeling of the expanding CME's leading edge, we indeed find a correspondence between the observed multiple type II drifting lanes and the shock signatures observed in the O VI spectral lines. Incidentally, this correspondence will cast new light on the nature of multiple lanes in the metric band, a topic that is still under debate (Shanmugaraju et al. 2005; Subramanian & Ebenezer 2006) and that has been thoroughly discussed for this same event by Reiner et al. (2007), who utilized both metric and kilometric radio dynamic spectra for their analysis, reaching a somewhat different conclusion. The joint analysis of the radio and UVCS spectra will eventually allow us to draw conclusions about ion heating and its dependence on upstream plasma parameters.

The paper is organized as follows. In § 2 we describe the 2002 July 23 CME event as observed by several instruments at different wavelengths. In § 3 an overview of the spectral data diagnostics and the main results of the multiwavelength data analysis and modeling are described. Finally, we discuss the results and give our conclusions in § 4.

2. OBSERVATIONS

The 2002 July 23 event was well covered by many space- and ground-based instruments. An intense X4.8 solar flare was observed with the *GOES* full-Sun X-ray monitors near the east limb in NOAA Active Region 0039 at latitude S12° and longitude E72°. According to Solar Geophysical Data reports, the emission began to rise at 00:18 UT and reached a peak at 00:35 UT, decaying until 00:47 UT. This energetic flare was also observed in hard X-ray wavelengths (Krucker et al. 2003), γ-ray wavelengths (Lin et al. 2003), microwaves (White et al. 2003), and even the UV, off the limb, with UVCS measurements of photons scattered from coronal O VI ions (Raymond et al. 2007).

The initial phase of the temporal evolution of the CME was detected by the *Transition Region and Coronal Explorer* (*TRACE*) spacecraft (Handy et al. 1999). During the event, *TRACE* was observing in the Fe XII 195 Å passband. The pixel size of the CCD was 1″ with a temporal resolution of about 9 s, and the field of view covered the entire active region responsible for the flaring emission.

Higher up in the corona, the UVCS was observing with an interrupted sequence of exposures designated for major flare watches above the active region from 22:31:07 UT on July 22 to 01:24:45 UT on July 23. The UVCS is a long-slit UV spectrograph consisting of two spectrometric channels for the observation of spectral lines in the UV range and a visible light channel for polarimetric measurements of the extended solar corona. The 40′ slit is placed parallel to a tangent to the solar limb and can be moved along the radial direction to observe the entire corona at heliocentric distances between 1.4 and 10 $R_\odot$. In order to cover all the possible position angles, the slit can be rotated by 360° about an axis pointing to the center of the Sun. The spectral observations considered here consist of 120 s exposures separated by about 10 s readout intervals providing the spectrum of the coronal region in the instantaneous field of view determined by the spectrometer entrance slit. At the time of the CME passage, the UVCS slit was placed near the east limb at a mirror height of 1.63 $R_\odot$ from the center of the Sun, with the point along the slit closest to the Sun at an angle of 96° from the north pole. The slit width was 100 μm, delivering a spectral resolution of ~0.4 Å and a spatial resolution of 28″ in the radial direction. In order to maximize spectral coverage within telemetry limitations, the data were binned to 42″ along the slit length. Five wavelength panels on the O VI detector covered a spectral range including the Lyβ, Lyγ, and Lyδ lines along with O I $\lambda\lambda$989, 991, [Si VIII] $\lambda\lambda$945, 949, [Si IX] λ950, C III λ977, N III $\lambda\lambda$990, 992, O VI $\lambda\lambda$1032, 1037, [Fe XVIII] λ974, and Si XII $\lambda\lambda$499, 521 in second order. Data calibration is described by Gardner et al. (2002).

Above the UVCS slit height, a very fast, eastward-propagating CME associated with the flare was first visible in difference images at 00:42 UT with the Large Angle and Spectrometric Coronagraph Experiment (LASCO; Brueckner et al. 1995) C2 instrument on board *SOHO*. LASCO C2 is a white-light coronal imager designed with a near-360° field of view covering heights from about 2.25 to 6.0 $R_\odot$. Figure 1 shows a composite image of the 2002 July 23 CME obtained by combining running difference images taken from the LASCO C2 (at 00:42 UT), Mk4 (at 16:50 UT on the previous day), and EIT Fe XII 195 Å (at 01:00 UT; not to scale). In the same figure, a previous image from the Mark-IV (Mk4) coronameter of the Mauna Loa Solar Observatory (MLSO; Elmore et al. 2003) coronagraph is overlapped in order to yield a better insight on the global structure of the pre-CME corona. Mk4 has a field of view from about 1.1 to 2.8 $R_\odot$ and acquires white-light images with a cadence of 3 minutes.

Shock-related metric type II radio emission was detected between about 00:28 and 00:52 UT by ground-based radio spectrometers located at Hiraiso (Japan) and Culgoora (Australia) and by three Radio Solar Telescope Network (RSTN) observatories operated by the US Air Force, located in Holloman (New Mexico), Palehua (Hawaii), and Learmonth (Australia). A global overview of the complex multilane metric radio emission associated with this event is displayed in the dynamic spectrum recorded by the Hiraiso Radio Spectrograph in the time interval 00:25–00:55 UT (Fig. 2). Metric radio emission related to the same event included a large group of type III bursts and type IV continuum radiation. Type III radio bursts are commonly interpreted as plasma emission at the local plasma frequency from beams of nonthermal electrons released during the impulsive phase of the flare and propagating at a few tenths of the speed of light along open magnetic field lines with energies in the range from a few to 100 keV. In this case, episodes of shock-associated type III emission from electron beams accelerated at the shock front are also visible in the dynamic spectra. A type IV frequency-drifting structure, due to electrons trapped in the magnetically confined (plasmoid) CME structure and emitting a combination of plasma and gyrosynchrotron emission, is also visible in the spectrum, starting at 1500 MHz at about 00:28 UT and drifting slowly toward the lower frequencies.

3. DATA ANALYSIS

3.1. *CME Ice Cream Cone Model*

In the projection of the sky, most of the CME events observed near the limb in white light expand radially as cone-shaped blobs with nearly constant angular widths as a function of height (Webb et al. 1997; Schwenn et al. 2005). The geometrical properties of such CMEs have been modeled accordingly (Howard et al. 1982; Zhao et al. 2002). From the analysis of LASCO observations, the 2002 July 23 CME does appear to belong to the above category (see Fig. 3). We thus modeled the observed eruption as a conically expanding bubble-type CME in which the apex of the cone is located at the center of the Sun, as in Mancuso & Raymond (2004) and Mancuso (2007). In this "ice cream cone" model, the swept-up coronal material composing the CME leading-edge surface is supposed to expand at a fixed angle that we assume coincides with the estimated CME width (~56°). Although the

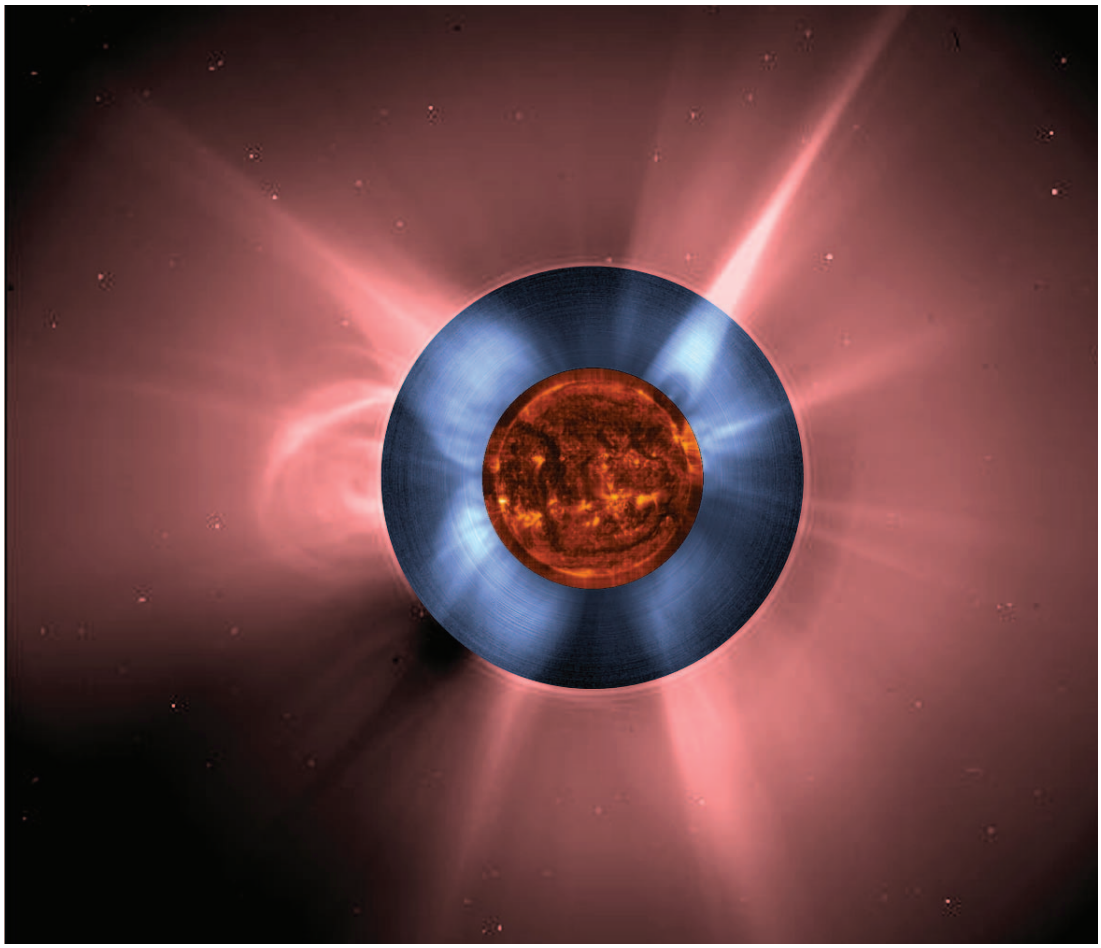

FIG. 1.—Composite image using a combination of running difference images taken from LASCO C2 (at 00:42 UT), Mk4 (at 16:50 UT on the previous day), and EIT Fe XII 195 Å (at 01:00 UT; not in scale) for the 2002 July 23 CME.

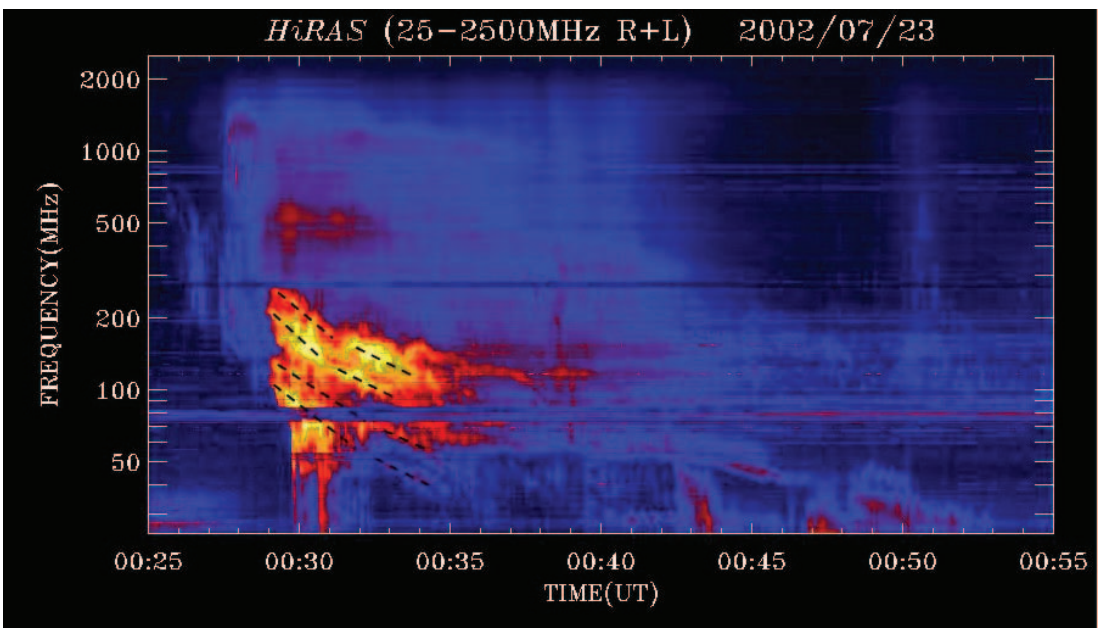

FIG. 2.—Dynamic spectrum of the 2002 July 23 event from 25 to 2500 MHz observed by the Hiraiso Radio Spectrograph during the period 00:25–00:55 UT. The dashed lines indicate the approximate locations of the two branches of the band-split patterns in the most prominent emission band.

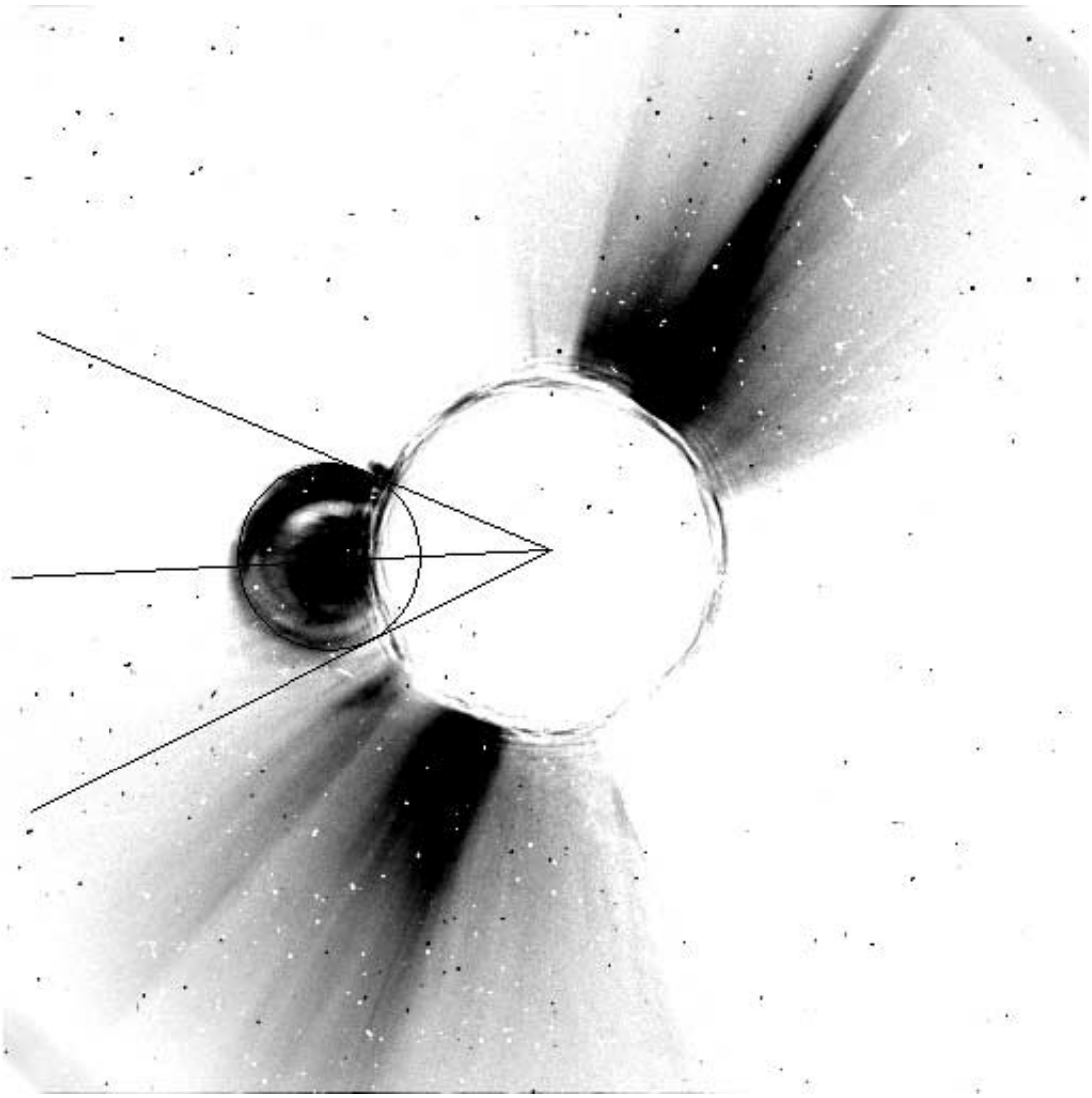

FIG. 3.—Negative of a running difference image from LASCO C2 (at 00:42 UT). The 2002 July 23 CME appears as a bubble propagating radially and maintaining its angular width nearly constant.

CME-driven shock should be spatially separated from the driver CME by a standoff distance, its dependence on heliocentric height is currently not known. Near the Sun, the expectation is that the shock is relatively close to the white-light CME (Vourlidas et al. 2003).

The propagation of the CME along its axis of symmetry (roughly perpendicular to the UVCS slit) was estimated from the available white-light and UV data by measuring the plane-of-the-sky heliocentric distance of its leading edge in units of solar radius. In Figure 4 we show the distance-time measurements obtained by the analysis of the available *TRACE*, UVCS, and LASCO C2 measurements. This information was used to infer the CME height-time trajectory (*solid line*) by least-squares fitting the available data with a cubic polynomial. The distance refers to the projection on the plane of the sky of the radial distance from the Sun center. Since the active-region group associated with the CME is near the limb, projection effects should not be important for this event. The absence of high (>100 km s^{-1}) Doppler shifts in the UVCS spectra during the initial detection of the CME confirms this expectation. The inset in Figure 4 shows the inferred sky-plane CME speed obtained by taking the time derivative of the cubic polynomial fit.

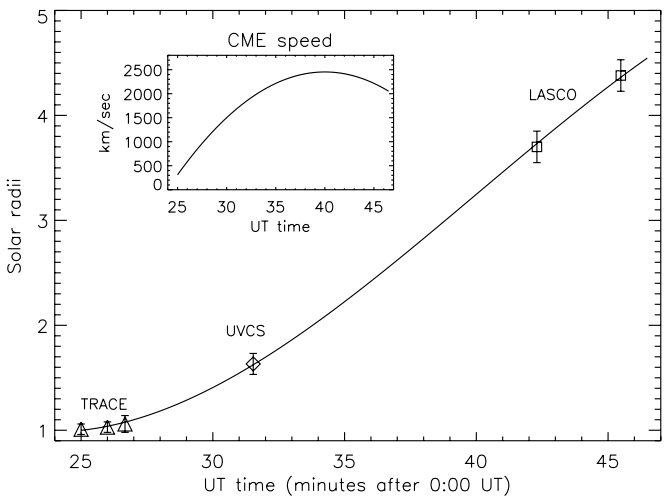

FIG. 4.—CME height-time trajectory (*solid line*) obtained by fitting the observed LASCO C2 and *TRACE* data (*squares and triangles*) with a cubic polynomial. The distance refers to the projection on the plane of the sky of the radial distance from the Sun center. The inset shows the CME speed obtained by taking the time derivative of the cubic polynomial fit.

The ice cream cone CME model described above, expanding at the rate imposed by the observational constraints, was used to build a synthetic metric dynamic spectrum for this event. We show that with a proper description of the CME kinematics, together with a refined coronal density profile, it is possible to replicate with excellent agreement the main lanes of the observed complex type II radio emission structures, implying that the shock sites are located just above the spherically expanding CME's leading edge, as expected for CME-driven shocks. Having verified the CME-driven origin of the shock and established the overall accuracy of the adopted geometrical model for the CME expansion, we show that the broad wings of the O VI spectral lines observed by UVCS, which will be analyzed later, are a result of shock-related thermal broadening and not of the bulk motion of the CME-expanding material along the line of sight. This allows us to discuss the effect of plasma parameters on ion heating.

3.2. *Synthetic Dynamic Spectrum*

The dynamic spectrum displayed in Figure 2 shows metric type II emission lanes at the fundamental and second harmonic, as well as band-splitting and herringbone structures (embedded type III radio bursts).

The fundamental band of the most prominent type II emission lane started at about 00:29 UT with a frequency of 110 MHz and was preceded and followed by flare- and/or shock-associated, fast-drifting type III radio bursts. The type II emission lanes drifted down to ~40 MHz in about 5 minutes, giving an average drift rate of approximately -0.23 MHz s^{-1}, and appear to be further split into two parallel lanes with a split ratio well below 2 (Fig. 2, *dashed lines*). Band splitting is not seen in every type II burst, and the mechanism is not yet fully understood. One plausible theory (Smerd et al. 1975) is that it is generated from plasma emission occurring from both upstream and downstream of the coronal shock front.

A slowly drifting (approximately -0.06 MHz s^{-1}) radio emission lane is also visible at later times, from about 00:37 to 00:50 UT. This type II–like emission lane is only apparently connected to the harmonic of the most prominent band previously discussed. In general, the nature of multiple lanes in the metric band is still under debate (Mancuso & Abbo 2004; Shanmugaraju et al. 2005; Subramanian & Ebenezer 2006; Reiner et al. 2007). It is possible that multiple metric type II emissions can originate from the ejection of additional coronal material associated with the flare/CME event. Alternatively, they may originate from a distinct blast-wave shock associated with the flare itself. We show instead that the two differently drifting emission lanes observed in the metric band on 2002 July 23 were produced by distinct portions of a single shock-wave surface piston-driven by the expanding CME.

In order to model the observed radio emission, that is, to convert the height-time data displayed in Figure 4 to the corresponding frequency-time relationship, we need to rely on a coronal electron density model. A multifold Newkirk (1961) model decaying with height as $\sim 10^{4.32/r}$ is widely used in order to interpret type II radio emission. This model, valid below about 2 $R_\odot$, is too simple for the range of heights considered here (e.g., Vršnak et al. 2004). For the interpretation of the dynamic spectrum of this same event, Reiner et al. (2007) used a Saito et al. (1970) model given by a combination of an $\sim r^{-6}$ *coronal* term and an $\sim r^{-2}$ *solar wind* term. This latter model, however, does not provide a smooth transition of $n_e(r)$ from the lower to the higher corona into the solar wind. A more accurate model would be one containing an additional $\sim r^{-16}$ term to describe the active region corona and an $\sim r^{-4}$ term for modeling a smoother transition in the region of interest (e.g., Mancuso & Spangler 2000). For the analysis of this event we used a combination of a formulation of the coronal electron density appropriate for solar maximum conditions from Bohlin & Garrison (1974), strictly valid above about 2 $R_\odot$, and a steeper Baumbach-Allen–like (Cox 2000) density profile at lower heights,

$$n_e(r) = \left(\frac{2.99}{r^{16}} + \frac{1.55}{r^{6}} + \frac{2.1}{r^{4}} + \frac{0.08}{r^{2.5}} \right) \times 10^8 \text{ cm}^{-3}. \quad (1)$$

The $\sim r^{-2}$ falloff of the interplanetary plasma electron density is not modeled, since we are interested in heliocentric distances well below 10 $R_\odot$.

The above radial density profile (multiplied by a factor of 1.2 in order to match the data) was used to convert the observed CME shock heights to the corresponding frequencies, according to the already-mentioned $f \propto (n_e)^{1/2}$ dependence. Figure 5 (*bottom*) shows the model dynamic spectrum superimposed on selected lanes of actual radio measurements (*asterisks*) extracted from the Learmonth radio dynamic spectrum (*top*) that displays frequencies from 25 to 180 MHz. The upper split bands were not plotted to avoid confusion. The measurements were obtained by using the software developed by J. Kennewell and colleagues at Learmonth, freely available for download from the NOAA National Geophysical Data Center Web site.[1] This Web site provides access to a number of space weather databases, including the RSTN solar radio spectral data used in this work. The solid lines in Figure 5 represent the frequencies emitted from a type II radio-emitting source propagating through the model density profile expressed by equation (1) along the axis of symmetry of the CME and just above the CME leading edge. The dashed lines represent the model frequencies that refer to type II emission by a source propagating at an angle of ~28° with respect to the axis of symmetry of the CME. The match between observed and model data is outstanding.

We thus conclude that a unique coronal density model, appropriate for a wide range of heliocentric heights and for solar maximum conditions, when applied to an appropriate dynamical evolution of the shock front, is able to replicate quite faithfully the observed radio dynamic spectrum without further assumptions. This result suggests that studying the nature of multiple type II emission lanes with overly simplistic density profiles or incomplete CME kinematic information, especially at the lower heliocentric heights involved in metric band emission, may be misleading and induce an erroneous interpretation (see Mancuso & Raymond [2004] and Mancuso [2007] for further discussion of this topic).

The 2002 July 23 shock was therefore CME-driven, with type II emission presumably located near both the top and the flanks of the expanding CME's leading edge. This information is of paramount importance in the following interpretation of the observed broadening of the O VI spectral lines.

3.3. *Fitting the* O VI *Spectral Lines*

We now consider the change in the O VI λ1032 spectral lines observed during the CME shock passage by UVCS. In general, the two major features observed in the UV spectra after the passage of a shock are the dimming and the broadening of the O VI spectral line profiles (e.g., Mancuso et al. 2002). The observed O VI emission is composed, in fact, of both a collisional and a radiative component that originate from the resonant scattering of the chromospheric line by the oxygen ions of the corona. As these ions move outward in the corona, this latter component dims

[1] See http://www.ngdc.noaa.gov.

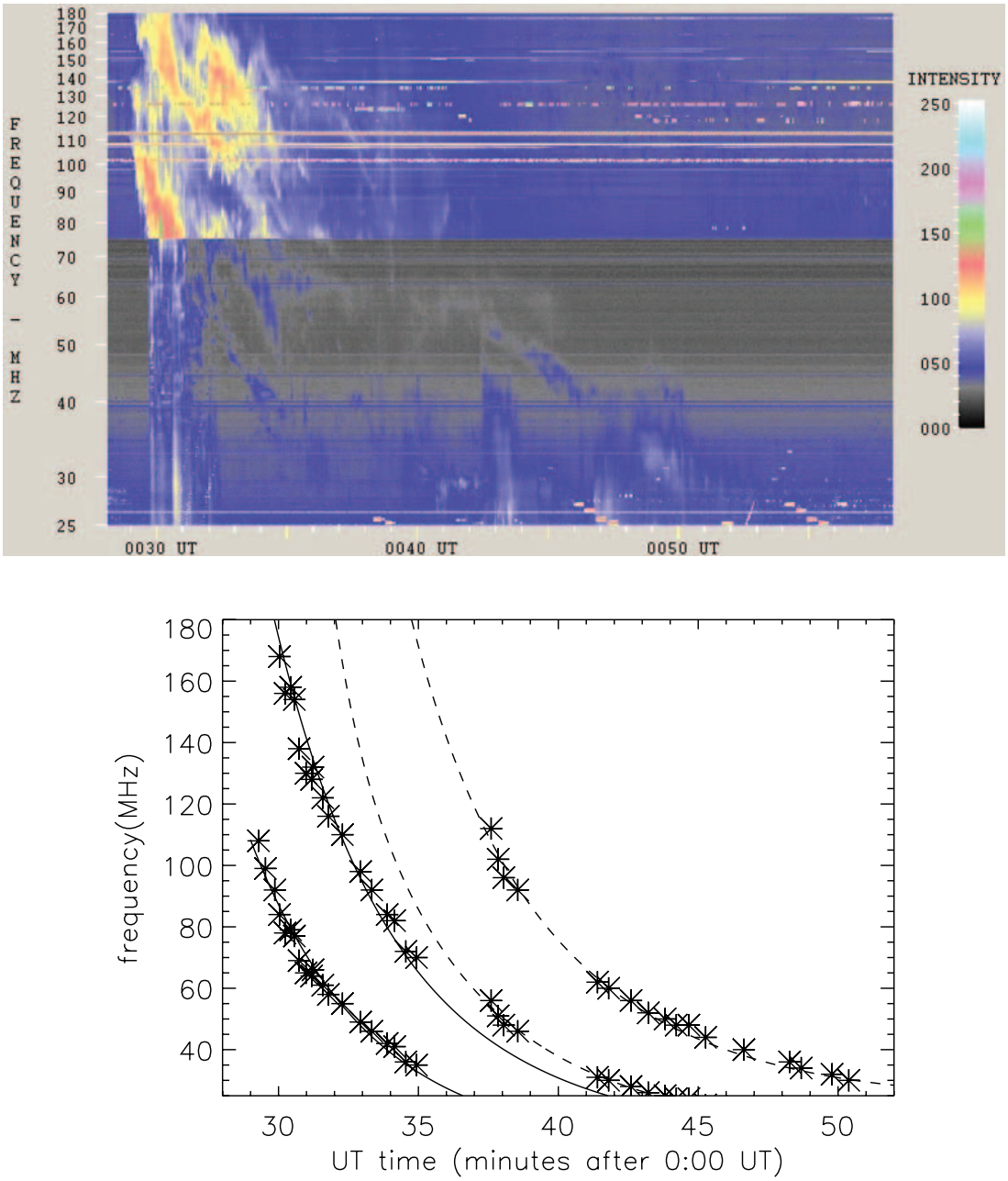

FIG. 5.—*Top*: Dynamic spectrum of the 2002 July 23 event from 25 to 180 MHz observed by the Learmonth radio spectrograph at 00:28–00:58 UT. *Bottom*: Model dynamic spectrum superimposed on actual radio measurements extracted from the above radio dynamic spectrum. The solid lines represent the frequency emitted from a source propagating through the model density profile expressed by eq. (1) along the axis of symmetry of the CME. The dashed lines represent the model frequency emitted by a source propagating at an angle of $\sim 28^{\circ}$ with respect to the axis of symmetry.

because the solar emission and coronal absorption profiles are Doppler-shifted apart. At the passage of a fast CME shock, the radiative component is practically washed out, since fewer particles are able to scatter the disk radiation and the O VI line intensities are thus expected to drop abruptly, unless the collisional component of the perturbed plasma is able to balance such an effect. Moreover, in the presence of a shock, the higher electron temperature in the shocked plasma excites O VI ions to higher ionization states, which further reduces the line intensities.

Both expansion of the emitting volume and enhanced temperature of the shocked plasma contribute instead to the broadening of the O VI line profiles. Line broadening of oxygen line profiles is expected from in situ measurements that show a larger heating of the less abundant ion species in the solar wind with respect to the protons downstream of an interplanetary shock (Berdichevsky et al. 1997). The downstream ion temperature can be several tens of times higher than that in the upstream region. Because of the prominent role of shock waves in accelerating solar energetic particles, and because UV spectra provide unique diagnostics for the physical processes in shocks, it is important to know whether the emission arose from shocked plasma.

The O VI λ1032 spectra taken from four 120 s exposures from 00:30:32 to 00:39:05 UT are shown in Figure 6 (*squares*), along with the respective fits (*solid lines*). The portion of the slit over which the observed flux was integrated at each exposure was chosen in order to match the location of the intersection of the CME leading edge with the slit. The insets in Figure 6 schematize the model expansion of the CME along the plane of the sky and

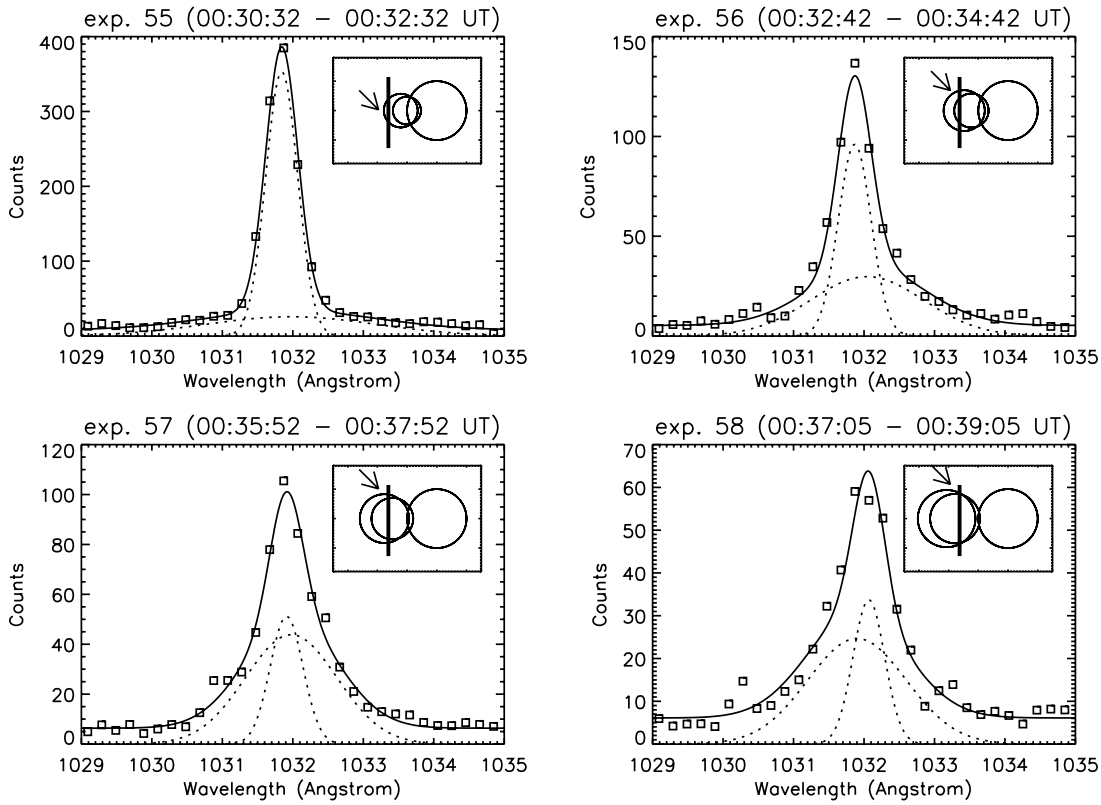

FIG. 6.— O VI λ1032 line profiles at the passage of the shock along the slit (*squares*). The solid lines show the results of the two-Gaussian fit (plus constant background) with a narrow and a broad profile (*dotted lines*). The insets depict the model expansion of the CME along the slit at the beginning and ending times of each of the 120 s exposures. The arrows indicate the approximate location along the slit where the spectra were obtained.

through the slit at the beginning and ending times of each of the 120 s exposures. The arrows indicate the approximate locations along the slit where the spectra plotted in Figure 6 were obtained. A summary of the observations can be found in Table 1, where we list the start and end times of the single exposures, the slit portions (in arcseconds) over which the spectra have been integrated, and the observed FWHMs of the broad components of the O VI λ1032 spectral lines.

After correcting for the instrument profile (Kohl et al. 1997), we used a two-Gaussian fit (plus a constant background) to separate the background corona emission (whose narrow component was fixed to the width of the pre-CME line profile) from the shock emission. As shown in Figure 6, the broad profile of the front overlaps the much brighter and narrower profile of the background corona. While the narrow component traces the almost undisturbed coronal material along the line of sight, the broad component is emitted by bulk motion and/or by the plasma that is expanding outward after being heated by the shock passage. Doppler shifts are generally small ($<$100 km s^{-1}), showing that the motion of gas is mostly transverse to the line of sight, as supposed.

Sudden brightening of spectral lines from heavy ions such as Si XII and [Fe XVIII] was also detected after the shock passage (see Raymond et al. 2003), indicating high electron temperatures and enhanced local collisional excitation. In particular, the brief episode of [Fe XVIII] emission lasting for two exposures near the northern end of the slit is unusual among the CMEs observed by UVCS and should not be related to the bright, narrow [Fe XVIII] emission features observed in other events by Ciaravella et al. (2002) and Ko et al. (2003), which have instead been attributed to current sheets beneath expanding flux ropes (e.g., Lin & Forbes 2000). The association of these enhanced heavy ion emission lines with a shock propagating in the northern portion of the UVCS slit is thus fairly likely, although the paucity of counts available for each exposure in the selected portions of the slit examined in this paper prevents conclusive analysis and further discussion on this topic.

3.4. *Bulk Motion or Thermal Broadening?*

CME shocks interact with the corona by heating and accelerating particles. The heating mechanisms and their dependencies on plasma parameters such as plasma β (i.e., the plasma-to-magnetic pressure ratio in the upstream region) and the mass-to-charge ratio are not well understood. Shocks can heat ions by transforming the ordered bulk kinetic energy of the flowing plasma into the random thermal energy of the particles. In ordinary fluids,

TABLE 1
SUMMARY OF UVCS OBSERVATIONS

Exposure	Start (UT)	End (UT)	Slit Portion (Lower End) (arcsec)	Slit Portion (Upper End) (arcsec)	$v_{\rm FWHM}^{\rm obs}$ (km s^{-1})
55.....	00:30:32	00:32:32	−210	210	830 ± 162
56.....	00:32:42	00:34:42	378	630	548 ± 69
57.....	00:34:52	00:36:52	588	840	446 ± 51
58.....	00:37:05	00:39:05	714	966	478 ± 72

collisions redistribute the energy among all particles, so that they have the same temperature. However, since the scale lengths of collisionless shocks are less than the mean free path between collisions, shock heating must use mechanisms unique to plasma, with instability-generated waves replacing collisions, so that the electrons and ions may not be heated by the same process.

The spectral profiles of the O VI λ1032 line presented in the previous section suggest the presence of thermal broadening due to the shock passage. Estimating the contributions of bulk motion in the observed line widths is, however, essential in order to yield a correct interpretation and allow a reliable comparison of the observations with theories on ion heating. The contributions of bulk motion can be estimated as follows. Each ion concurs with the detected line profile with a speed that depends on its position along the front. If the thickness of the bubble is small, as probably is the case for CME fronts, and the spectral resolution is high or the expansion speed is very large, the two components from the front and back sides of the shell will be detected as separate lines (Raymond et al. 2003). Otherwise, as for the present event, broadening of the line is seen. Assuming the validity of the model presented in the previous section, that is, a CME bubble expanding along a cone with an axis of symmetry along the plane of the sky and origin at the center of the Sun, an upper limit to the full width at half-maximum (FWHM) was estimated (Ciaravella et al. 2006) as

$$v_{\rm FWHM}^{\rm upper} < \int\int 2v_{\rm exp} \sin\theta \cos\phi \, d\theta \, d\phi, \qquad (2)$$

where $v_{\rm exp}$ is the expansion speed of the CME bubble, θ is the angle between the vertical and the line connecting the CME site along the leading edge to the intersection of the line of sight with the bubble, and ϕ is the azimuthal angle such that $\cos\phi = 1$ along the line of sight.

Applying the above formula, the maximum FWHM due to the bulk expansion speed through the slit center (exposure 55) is $v_{\rm FWHM}^{\rm upper} = 574$ km s^{-1}. This latter should be considered a generous upper limit on the true value in that, within the 120 s exposure time, we do not know when the front enters the slit, while in the above calculation we supposed that the CME leading edge enters the slit exactly at the beginning of the exposure. The width derived from the fit of the broad O VI component centered at time 00:31:32 UT (Fig. 6, *top left*) yields 830 $\pm$ 162 km s^{-1}. Even taking into account that part of the broadening is due to CME bulk motion, we find, by subtracting in quadrature, a contribution from shock heating of $\sim$600 km s^{-1}.

In the following exposures (56–58), the contribution from bulk motion will be considerably less due to the geometry involved in Figure 6. For exposure 56, for example, which was taken in the interval between 00:32:42 and 00:34:42 UT (see Table 1), the upper limit to the bulk motion contribution will be a mere 253 km s^{-1}, much less than the observed 548 $\pm$ 69 km s^{-1}. Again, subtracting the bulk motion contribution in quadrature will yield $\sim$500 km s^{-1} for the shock contribution. As for the following two exposures (57 and 58), it is clear from Figure 6 that the bulk motion contribution along the UVCS slit will be even smaller.

Comparing the $v_{\rm FWHM}^{\rm upper}$ computed from equation (2) with the fitted $v_{\rm FWHM}^{\rm obs}$ of the O VI line broad components, we thus conclude that the broad components of the O VI lines observed along the slit during the CME shock passage are mostly attributable to thermal broadening of shocked plasma, and that, subtracting in quadrature the modeled bulk motion contribution, the FWHMs due to thermal broadening can be grossly estimated at around 500–600 km s^{-1}.

4. DISCUSSION AND CONCLUSIONS

With respect to the shocks observed by Raymond et al. (2000) and Mancuso et al. (2002), who found O VI line widths near $(3/4)v_{\rm shock}$ for $\sim$1000 km s^{-1} coronal shocks, this event shows line widths that lie around $\sim$30% of the estimated radial shock speed ($\sim$1700 km s^{-1} at 1.63 $R_\odot$).

It must be recognized that line widths of order $(3/4)v_{\rm shock}$ are expected only for idealized flows at large Alfvénic Mach numbers ($M_{\rm A}$, defined as the shock speed divided by the Alfvén speed). This condition is never met in the case of coronal shocks, which instead present fairly low Alfvénic Mach numbers. In addition, wave-particle interactions and the effect of plasma parameters such as plasma β and the mass-to-charge ratio play a crucial role in the heating of heavy ions (e.g., Korreck et al. 2007). Our result is probably suggestive of a different ion-heating mechanism operating in the present event with respect to the ones acting on the plasma heated by previous CME shock events examined by UVCS.

A possible explanation may arise from the consideration that this particular event was propagating through relatively high coronal plasma β, a fact that is known to affect ion heating. Information on the physical parameters of upstream plasma can actually be inferred from radio spectrograph data. While describing the radio dynamic spectrum for this event, we already mentioned the presence of band-splitting in the emission lanes. This wide splitting ($\sim$20 MHz around the time of the shock passage through the UVCS slit) implies strong compression *if* the band split is interpreted as due to plasma emission from the upstream (emitted at $f = f_l$) and downstream (emitted at $f = f_u > f_l$) shock regions (Smerd et al. 1975; Cho et al. 2007). In general, there is no certainty that the two parallel emission lanes are the result of band-splitting rather than, for instance, the effect of two radio sources located along the shock front. However, a few selection criteria may help in deciding between the above two options. Specifically, two lanes can be considered "split" if they show a frequency ratio other than 2, synchronized frequency time evolution, and similar intensity fluctuations (e.g., Vršnak et al. 2001). All of these criteria appear to be satisfied for the present event: the observed split ratio is well below 2, both split lanes drift at a similar rate, and they appear to start simultaneously, dimming and intensifying in fair agreement (see Fig. 2).

Bearing in mind that $f \propto (n_e)^{1/2}$, the compression ratio at the shock front can be expressed as $X = n_2/n_1 = (f_u/f_l)^2$, where n_2 and n_1 are the downstream and upstream plasma densities, respectively. The mean value of the compression ratio and its dispersion about the mean in a time interval around the UVCS observations (from about 00:30 to 00:36 UT) were determined by averaging the instantaneous compression ratios of a set of split emission patches (taken at discrete times, roughly equidistant in time) from both the fundamental and harmonic lanes of the most prominent emission. The result, $X = 2.2 \pm 0.1$, implies strong compression behind the shock front. Usually, compression factors below 2 are expected for coronal shocks (Mann et al. 1995). Assuming perpendicular propagation (dissipation for perpendicular shocks is more efficient than for parallel shocks), the Alfvénic Mach number can thus be expressed as $M_{\rm A} = [X(X + 5 + 5\beta)/2(4 - X)]^{1/2}$ (Vršnak et al. 2002), yielding $M_{\rm A} = 2.4 \pm 0.1$, a value that identifies this shock as supercritical (Kennel 1987). For subcritical shocks, the heating is spatially local to the shock front via conduction, while supercritical shock dissipation of energy is based on multiple streams of ions with longer characteristic scales. Plasma β is defined by the plasma-to-magnetic pressure ratio in the upstream region; i.e., it is related to the Alfvén

and sound speed by $\beta = 8\pi n k_B T/B^2 = 2c_s^2/\gamma v_A^2$. Here $v_A = B/(4\pi n \mu m_p)^{1/2}$ is the Alfvén speed, $c_s = (\gamma k_B T/\mu m_p)^{1/2}$ is the sound speed, m_p is the proton mass, $\gamma = 5/3$ is the ratio of the specific heats, k_B is Boltzmann's constant, and $T \sim 1.4 \times 10^6$ K (Raymond et al. 2003) is the temperature. The electron number density n_e is related to the full particle number density n by $n \sim 1.92 n_e$ for a mean molecular weight $\mu = 0.6$ (Priest 1982). An average functional form of the magnetic field radial profile, valid between about 1.5 and 2.3 $R_\odot$, was given by Mancuso et al. (2003) as $B(r) = 0.6(r-1)^{-1.2}$ G, where r is the radial distance in units of solar radii. Taking the value of the density n_e at 1.63 $R_\odot$ deduced from equation (1), we obtain $\beta \sim 0.4$. For comparison, the plasma β estimated for the 2000 March 3 shock was half this value (Mancuso et al. 2002).

For supercritical interplanetary shocks, Korreck et al. (2007) showed that with increasing β the heating of ions tends to decrease by several factors. This implies that ion heating is more effective in magnetically dominated regimes or, alternatively, in comparatively less dense regions. Dependence on the Alfvénic Mach number is less clear (Schwartz et al. 1988) and should not be a major issue here. Our result thus suggests that there might be a deficiency of ion heating in the present event with respect to what was observed in previous CME shocks detected by UVCS, and that this deficiency might be attributable to different local plasma conditions, such as higher plasma β. Higher coronal plasma density is expected during the advanced maximum phase of the solar cycle, as in the present case. The present result thus supports the findings of Korreck et al. (2007) on the dependence of ion heating on the plasma β parameter.

In summary, we found that a unique coronal density model appropriate for a wide range of heliocentric heights and for solar maximum conditions, when applied to an appropriate dynamical evolution of the shock front, is able to replicate quite faithfully the observed complex radio dynamic spectrum without further assumptions. Multiple type II emission lanes in the metric band therefore result, at least in this case, from a different portion of an expanding CME-driven shock surface propagating just ahead of the CME and *not* from different ejecta and/or blast waves. This result suggests that trying to infer the origin of multiple type II emission lanes with overly simplistic density profiles or incomplete CME kinematic information, especially at the lower heliocentric heights involved in metric band emission, may be misleading and induce erroneous interpretations. The above analysis implies that the shock was indeed CME-driven and that the model CME expansion and the coronal density used here were fairly reliable. This knowledge allowed us to better discriminate between bulk motion and thermal broadening contributions in the shape of the observed O VI spectral lines. Finally, our result suggests that plasma β could be an important parameter in determining the effect of ion heating at collisionless shock fronts, as shown by Korreck et al. (2007) for interplanetary shocks, even in the coronal environment.

SOHO is a project of international cooperation between ESA and NASA. The Mauna Loa Solar Observatory (MLSO) is operated by the High Altitude Observatory (HAO), a division of the National Center for Atmospheric Research (NCAR), which is sponsored by the National Science Foundation (NSF).

REFERENCES

Bale, S. D., Reiner, M. J., Bougeret, J.-L., Kaiser, M. L., Krucker, S., Larson, D. E., & Lin, R. P. 1999, Geophys. Res. Lett., 26, 1573
Berdichevsky, D., Geiss, J., Gloeckler, G., & Mall, U. 1997, J. Geophys. Res., 102, 2623
Bohlin, J. D., & Garrison, L. M. 1974, Sol. Phys., 38, 165
Brueckner, R. A., et al. 1995, Sol. Phys., 162, 357
Cairns, I. H. 1986, Publ. Astron. Soc. Australia, 6, 444
Cho, K.-S., Lee, J., Gary, D. E., Moon, Y.-J., & Park, Y. D. 2007, ApJ, 665, 799
Ciaravella, A., Raymond, J. C., & Kahler, S. W. 2006, ApJ, 652, 774
Ciaravella, A., Raymond, J. C., Kahler, S. W., Vourlidas, A., & Li, J. 2005, ApJ, 621, 1121
Ciaravella, A., Raymond, J. C., Li, J., Reiser, P., Gardner, L. D., Ko, Y.-K., & Fineschi, S. 2002, ApJ, 575, 1116
Cox, A. N. 2000, Allen's Astrophysical Quantities (4th ed.; New York: AIP)
Elmore, D. F., Burkepile, J. T., Darnell, J. A., Lecinski, A. R., & Stanger, A. L. 2003, Proc. SPIE, 4823, 66
Gardner, L. D., et al. 2002, in The Radiometric Calibration of *SOHO*, ed. A. Pauluhn, M. C. E. Huber, & R. von Steiger (ESA SR-002; Noordwijk: ESA), 161
Gopalswamy, N. 2006, in Solar Eruption and Energetic Particles, ed. N. Gopalswamy, R. Mewaldt, & J. Torsti (Geophys. Monogr. 165; Washington: AGU), 207
Handy, B. N., et al. 1999, Sol. Phys., 187, 229
Howard, R. A., Michels, D. J., Sheeley, N. R., Jr., & Koomen, M. J. 1982, ApJ, 263, L101
Kennel, C. F. 1987, J. Geophys. Res., 92, 13427
Knock, S. A., Cairns, I. H., Robinson, P. A., & Kuncic, Z. 2001, J. Geophys. Res., 106, 25041
Ko, Y.-K., Raymond, J. C., Lin, J., Lawrence, G., Li, J., & Fludra, A. 2003, ApJ, 594, 1068
Kohl, J. L., et al. 1995, Sol. Phys., 162, 313
———. 1997, Sol. Phys., 175, 613
Korreck, K. E., Zurbuchen, T. H., Lepri, S. T., & Raines, J. M. 2007, ApJ, 659, 773
Krucker, S., Hurford, G. J., & Lin, R. P. 2003, ApJ, 595, L103
Lin, J., & Forbes, T. R. 2000, J. Geophys. Res., 105, 2375
Lin, J., Mancuso, S., & Vourlidas, A. 2006, ApJ, 649, 1110
Lin, R. P., et al. 2003, ApJ, 595, L69
Mancuso, S. 2007, A&A, 463, 1137
Mancuso, S., & Abbo, L. 2004, A&A, 415, L17
Mancuso, S., & Raymond, J. C. 2004, A&A, 413, 363
Mancuso, S., Raymond, J. C., Kohl, J., Ko, Y.-K., Uzzo, M., & Wu, R. 2002, A&A, 383, 267
———. 2003, A&A, 400, 347
Mancuso, S., & Spangler, S. R. 2000, ApJ, 539, 480
Mann, G., Classen, T., & Aurass, H. 1995, A&A, 295, 775
Newkirk, G. J. 1961, ApJ, 133, 983
Priest, E. R. 1982, Solar Magneto-hydrodynamics (Dordrecht: Reidel)
Raouafi, N.-E., Mancuso, S., Solanki, S. K., Inhester, B., Mierla, M., Stenborg, G., Delaboudinière, J. P., & Benna, C. 2004, A&A, 424, 1039
Raymond, J. C., Ciaravella, A., Dobrzycka, D., Strachan, L., Ko, Y.-K., Uzzo, M., & Raouafi, N.-E. 2003, ApJ, 597, 1106
Raymond, J. C., Holman, G., Ciaravella, A., Panasyuk, A., Ko, Y.-K., & Kohl, J. 2007, ApJ, 659, 750
Raymond, J. C., et al. 2000, Geophys. Res. Lett., 27, 1439
Reiner, M. J., Krucker, S., Gary, D. E., Dougherty, B. L., Kaiser, M. L., & Bougeret, J.-L. 2007, ApJ, 657, 1107
Saito, K., Makita, M., Nishi, K., & Hata, S. 1970, Ann. Tokyo Astron. Obs., 12, 51
Schwartz, S. J., Thomsen, M. F., Bame, S. J., & Stansberry, J. 1988, J. Geophys. Res., 93, 12923
Schwenn, R., dal Lago, A., Huttunen, E., & Gonzalez, W. D. 2005, Ann. Geophys., 23, 1033
Shanmugaraju, A., Moon, Y.-J., Cho, K.-S., Kim, Y.-H., Dryer, M., & Umapathy, S. 2005, Sol. Phys., 232, 87
Sime, D. G., & Hundhausen, A. J. 1987, J. Geophys. Res., 92, 1049
Smerd, S. F., Sheridan, K. V., & Stewart, R. T. 1975, Astrophys. Lett., 16, 23
Subramanian, K. R., & Ebenezer, E. 2006, A&A, 451, 683
Vourlidas, A., Wu, S. T., Wang, A. H., Subramanian, P., & Howard, R. A. 2003, ApJ, 598, 1392
Vršnak, B., Aurass, H., Magdalenić, J., & Gopalswamy, N. 2001, A&A, 377, 321
Vršnak, B., Magdalenić, J., Aurass, H., & Mann, G. 2002, A&A, 396, 673
Vršnak, B., Magdalenić, J., & Zlobec, P. 2004, A&A, 413, 753
Webb, D. F., Kahler, S. W., McIntosh, P. S., & Klimchuck, J. A. 1997, J. Geophys. Res., 102, 24161
White, S. M., Krucker, S., Shibasaki, K., Yokoyama, T., Shimojo, M., & Kundu, M. R. 2003, ApJ, 595, L111
Zhao, X. P., Plunkett, S. P., & Liu, W. 2002, J. Geophys. Res., 107, 1223